Interfacial properties and functionality of hemp protein and carrageenan complexes at oil-water interfaces

MSc Thesis

Yuying Pang (1207393)

Supervisor: Xingfa Ma

Examiners: Leonard Sagis and Mehdi Habibi

Submitted on: 14-05-2024

Abstract

Emulsions play a crucial role in various food products, and proteins are commonly used to stabilize them. However, plant proteins, including hemp proteins (HPI), face challenges in emulsification due to their poor solubility compared to animal proteins. To improve their solubility, HPI can be electrostatically complexed with κ-carrageenan (KC) to enhance its emulsifying properties. This study investigated the oil-water interfacial properties of HPI and HPI-KC complexes at a ratio of 1:1, 0.5:1, and 0.25:1 and their emulsion stabilization. We first characterized the protein compositions by SDS-PAGE and measured the particle size and zeta potential of HPI and HPI-KC complexes. Results of SDS-PAGE showed the composition of HPI including 7S vicilin-like protein, edestin and albumin. Then, 0.25:1 complex showed both the highest particle size and absolute zeta potential. Automatic drop tensiometer (ADT) was then used to study the oil-water interfacial adsorption behavior and interfacial dilatational rheology. The resultant data from ADT was analyzed by Lissajous plots and a general stress decomposition (GSD) methodology. Results showed that HPI-KC complexes formed stiffer oil-water interfaces than HPI in response to dilatational deformation , where the 0.5:1 complex exhibited the highest interfacial stiffness. Finally, emulsions of HPI and HPI-KC complexes were prepared at 0.1 wt%, 0.3 wt% and 0.5 wt% and the storage stability was evaluated over 28 days. Emulsions stabilized with 0.5:1 and 0.25:1 complexes at both 0.3 wt% and 0.5 wt% showed smaller oil droplets and better dispersion. After 28 days, the emulsions stabilized with 0.5:1 and 0.25:1 ratio were more stable against coalescence than the ones with HPI and 1:1 ratio. These findings offer valuable insights for enhancing the effectiveness of hemp protein as emulsifiers by adding polysaccharide in creating stable emulsions, which can promote their potential applications in food products.

1. Introduction

Emulsion-based food, such as milk, cream, and desserts, play a crucial role in the food industry and in the sensory experience of consuming various food products. Proteins are often used as emulsifiers to stabilize O/W emulsions due to their amphiphilic properties, where the hydrophobic groups in the protein structure can drive proteins to diffuse to and adsorb at the oil-water interface and stabilize emulsions through electrostatic and steric repulsions (Lima et al., 2023). Driven by the need for more sustainable and nutritious food to feed the growing populations, a shift towards "sustainable diets" is encouraged (Rawal et al., 2024). In this scenario, with the increasing awareness of sustainability and the growing demand for natural ingredients, the potential of plant proteins as food emulsifiers has received increasing attention (Chen et al., 2023).

Hemp protein isolate (HPI) stands out for its notable essential amino acid composition among plant-based protein sources (Gholivand et al., 2024), with a far higher Arg/Lys ratio than many well-known protein sources, such as soy protein and casein (N. Wang et al., 2024). Hempseed protein does not require to be labeled as a priority allergen as compared to soy, pea, and milk proteins due to its hypo-allergenicity (Julakanti et al., 2023). Hempseed contains very low concentrations of nutrition absorption inhibitors or allergic compounds such as phytic acid, trypsin inhibitors, and condensed tannins, thus making it an excellent substitute for milk, pea, and soy products (Julakanti et al., 2023). Besides lower allergenicity, it also has a higher digestion rate, and nutritional characteristics (N. Wang et al., 2024).

However, plant proteins are promising sources of natural emulsifiers but are not yet widely used as emulsifiers because they have poorer emulsifying properties than animal proteins (Tang, 2017). Animal proteins are highly soluble in aqueous solutions, and adsorb readily at both air–water and oil–water interfaces. However, commercial plant-based protein extracts are often less soluble and less surface active (L. M. Sagis & Yang, 2022). The high hydrophobicity of plant proteins poses challenges in achieving optimal amphiphilic properties for interfacial stabilization. Therefore, they may not effectively coat oil droplets and cause aggregation.(Gholivand et al., 2024). For HPI, its poor aqueous solubility is a primary concern among the functional properties, as proteins must be in soluble form to

exhibit their desired functional features (Karabulut et al., 2024). The poor techno-functionality of hemp protein may affect its potential to be used in the food industry. Based on the above information, plant-based proteins have good potential as natural emulsifiers, but at acidic pH, they have to be modified (physically, chemically, or enzymatically) before they function effectively (McClements et al., 2017).

Hemp protein has a low solubility at acidic pH, therefore, we need to employ a method to enhance the functionality of hemp protein as emulsifiers. In this study, we will use polysaccharide to electrostatically complex with hemp protein. Complexing proteins with polysaccharides, dextrans or sugars can increase the solubility of protein at acidic pH and hence enhance emulsifying properties (Day et al., 2022). The behavior of aqueous mixtures of proteins and polysaccharides depends on the type of interactions between the two types of biopolymers. Plant protein and polysaccharide complexes associated by electrostatic interactions at acidic pH, which may increase the solubility of plant protein at acidic pH (Lima et al., 2023). Additionally, the complexation of protein with polysaccharide can form thick interfacial films and may greatly minimize contact with the droplets and exert steric repulsions between droplets (Dickinson & Galazka, 1991). Association is often driven by opposite charge interactions, though dipole-dipole or hydrophobic interactions may also play a role. The net charge of proteins varies from strongly negative at high pH to strongly positive at low pH with a net zero charge at their isoelectric point (pI). Therefore, opposite charge driven association of proteins with anionic polysaccharides such as k-carrageenan occurs at pH < pI and with cationic polysaccharides such as chitosan at pH > pI (Chassenieux & Nicolai, 2023). The typical range of pI for hemp proteins is 4.5–5 (Do et al., 2024). Compared to protein films, protein-polysaccharide films may have better resistance to environmental stresses such as major changes in pH, thermal processing, or freezing (Lima et al., 2023).

On the other hand, the addition of polysaccharides may also lead to instability of the emulsion. The formation and stability of dispersed colloidal systems depend on the environmental conditions (i.e., pH, temperature, ionic strength), concentration, and biopolymer ratios (Cheng et al., 2015). The concentration of polysaccharide used significantly influences the stability of multilayer oil-in-water emulsions. Insufficient polysaccharide concentrations or excessive amounts can lead to instability in

the droplets, caused by either bridging or depletion flocculation, respectively. However, when the polysaccharide is present at an appropriate concentration, the emulsions achieve stability due to the strong electrostatic and steric repulsions among the droplets (Tian et al., 2021). κ-carrageenan (KC) is a linear polysaccharide with one sulfate group in each repeating sugar unit, consisting of α-(1-3)-D-galactopyranose and β-(1-4)-3,6-anhydro-D-galactopyranose (Li et al., 2024). It is one of the most common hydrocolloids used in emulsion systems along with proteins in order to improve emulsion stability (Gholivand et al., 2024).

This study aims to investigate the effectiveness of κ-carrageenan in improving the interfacial properties and emulsion functionalities of hemp proteins. In this study, we compared the interfacial and emulsion properties of HPI with HPI-KC complexes at a ratio of 1:1, 0.5:1, 0.25:1. First, we characterized the complexes by measuring their particle size and zeta potential. Secondly, we measured the interfacial properties of HPI and complexes by automatic drop tensiometer. Lastly, we used HPI and complexes to make emulsions and measured the emulsion properties. The findings of this study provide comprehensive insights into enhancing the emulsification efficacy of plant protein emulsifiers, allowing for a better understanding of the types of foods they could potentially be applied to.

2. Materials and methods

2.1 Materials

Hemp flour was purchased from De Notenshop (Netherlands). κ-Carrageenan (KC) was purchased from Sigma-Aldrich (USA). All other chemicals (Sigma-Aldrich, USA) in this study were used as received. Ultrapure water (MilliQ Purelab Ultra, Germany) was used for all experiments unless otherwise stated.

2.2 Extraction of hemp protein isolate (HPI)

Hemp protein was extracted by dispersing the flour in an alkaline solution around pH 9.0, as the protein solubility increased at alkaline pH. The flour slurry was centrifuged at 13,000 rpm for 10 min, and hereafter the pellet containing carbohydrates and insoluble proteins was discarded, and the pH of supernatant was adjusted to around 4.6 to precipitate globulins, for 90 min. The protein suspension was

centrifuged at 13,000 rpm for 5 min, and then the pellet containing globulins was collected, followed by washing the pellet three times using MilliQ water. The precipitated globulin was redispersed in MilliQ water and then adjusted pH to 8.0. Lastly, the redispersed solution was dialyzed using dialysis tubing to remove free phenols, small sugars, and salts before freeze-drying. The protein extract was freeze-dried and stored at 4 ◦C for further analysis.

2.3 Extracted HPI characterization

The composition of extracted hemp protein isolate was characterized by sodium dodecyl sulfate polyacrylamide gel electrophoresis (SDS-PAGE). HPI were dispersed in water and pH 4.0 acetate buffer at 0.1 wt% protein concentration respectively, and 45 μL of each sample solution was mixed with 6 μL of 500 mM DTT and 7 μL of NuPAGE LDS sample buffer. Subsequently, these samples were heated to 70 ◦C for 10 min, and 15 μL of each sample was loaded on a 4–12% (w/w) BisTris gel. The included marker had a molecular weight of 2.5–200 kDa. Electrophoresis was performed in a XCell Surelock Mini-Cell for 30 min at 200 V. Afterwards, the gel was stained with SimplyBlue SafeStain and scanned with a Biorad GS900 gel scanner. In addition, the solubility of HPI from pH 7.0 to 3.0 was determined by Dumas.

2.4 Preparation of HPI and HPI-KC complex solutions

Preparation of 0.1 wt% HPI solution: 0.2 wt% HPI was first dispersed in 20 mM pH 4.0 acetate buffer at a constant stirring rate for 3 h. The HPI solution was then filtered to remove precipitates. These steps were repeated when preparing 0.3 wt% and 0.5 wt% HPI solutions.

For HPI-KC complexes, 0.2 wt% HPI and 0.2 wt% κ-carrageenan were dispersed in MilliQ water respectively, before stirring for 3 h at room temperature. After filtrating the HPI solution and κ-carrageenan solution, the were mixed at ratios of 1:1, 0.5:1, and 0.25:1. They were diluted to pH 4.0 with 40 mM acetate buffer and stirred for 1 h to ensure uniformity. These steps were repeated for the preparation of 0.3 wt% and 0.5 wt% HPI-KC complexes.

2.5 Particle size distribution

A Zetasizer Nano ZS (Malvern Instrument, UK) instrument was used to measure the nanoemulsions' droplet size and droplet size distribution at 20 ◦C. Measurements were performed in triplicate.

2.6 Zeta potential

The zeta potential of proteins in 20 mM sodium phosphate buffer was analyzed by dynamic light scattering using the Zetasizer Nano ZS (Malvern Instrument, UK). Before analysis, the HPI and KC solution were filtered on a 0.45 μm and 0.80 μm membrane to remove large contaminants. The refractive indices of the aqueous phase and protein were 1.33 and 1.45, respectively. Measurements were performed in triplicate at 20 ◦C.

2.7 Dilatational rheology

The oil-water interfacial dilatational rheology of 0.1 wt% HPI solution and HPI-KC complexes were measured by Automatic drop tensiometer (ADT), which characterized the mechanical properties of the complex interface in response to dilatational deformation. Amplitude sweeps and frequency sweeps were measured at least in triplicate at 20 ◦C. Lissajous plots and general stress decomposition (GSD) were used to analyze data of amplitude sweeps. GSD was applied using a MATLAB (R2020b) script (de Groot et al., 2023).

2.8 Preparation of emulsions

Emulsions were prepared by mixing HPI and HPI-KC complexes solutions (0.1 wt%, 0.3 wt%, and 0.5 wt%) with 10 wt% MCT oil using a high-speed blender (UltraTurrax, IKA, Staufen, Germany) at 12,000 rpm for 2 min. The coarse emulsions were then passed through a GEA high-pressure homogenizer (Niro Soavi NS 1001 L, Parma, Italy) for ten cycles at 180 bar.

2.9 Microscopic observation

The microstructure of emulsions was photographed under an Axioskop 2 Plus microscope (Zeiss

Axioskop 2 Plus) at 40 x magnification. For this purpose, a very thin layer of sample was placed onto a microscope slide. The slide was then covered with a lid at 20 ◦C to start the recording process.

2.10 Storage stability of emulsions

The droplet size distribution of emulsions was characterized by static laser light scattering (Malvern Instruments, Ltd, Worcestershire, UK). The droplet size of the emulsions was first measured in water and then again after mixing the emulsions with 1 wt% SDS solution at a 1:1 (v/v) ratio, to check for flocculation of the droplets. The emulsions were stored at room temperature for one month and the $D_{4,3}$ of the emulsions was monitored during storage. The flocculation and coalescence stability of the emulsions were evaluated by calculating the flocculation and coalescence index respectively, according to the following equations:

$$Flocculation\ index\ (\%) = \frac{D_{4,3}\ in\ water - D_{4,3}\ in\ SDS}{D_{4,3}\ in\ SDS} \times 100$$

$$Coalescence\ index\ (\%) = \frac{(D_{4,3}\ in\ SDS)_{-storage} - (D_{4,3}\ in\ SDS)_{-\ day\ 1}}{(D_{4,3}\ in\ SDS)_{-\ day\ 1}} \times 100$$

3. Results and discussion

3.1Characterization of HPI and HPI-KC complexes

3.1.1 Composition of HPI

The SDS-PAGE profiles of HPI that dissolved in pH 4.0 acetate buffer and MiliQ water in the presence and absence of reducing agent β-mercaptoethanol (2-ME) are shown in Fig. 1.

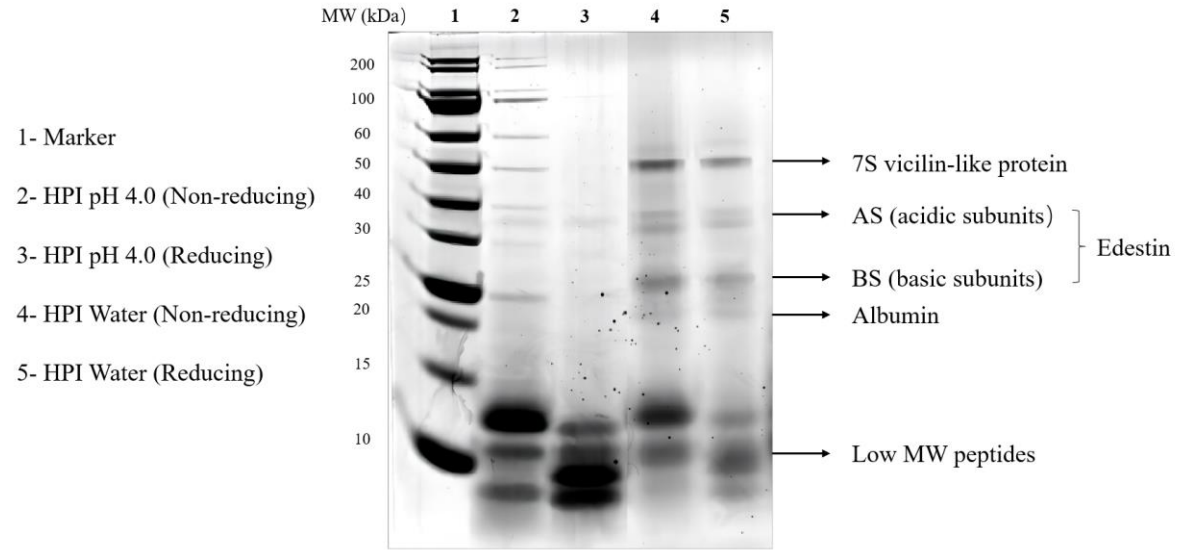

Fig.1. SDS-PAGE profile under non-reducing (lane 2, 4) and reducing (lane 3, 5) conditions containing Marker (lane 1; the corresponding molecular weights are indicated on the left), HPI dissolved in pH 4.0 acetate buffer (lane 2, 3), and water (lane 4, 5).

Hempseed proteins include a kind of legumin, so-called “edestin”. When HPI dissolved in water (lane 4, 5), there were two major kinds of edestin constituents, corresponding to acidic and basic subunits (AS and BS) of edestin, respectively (X. S. Wang et al., 2008). It can be seen that AS and BS had molecular weights (MW) of about 33.0 and 25.0 kDa, and the BS was more heterogeneous than the AS. Patel, Cudney, and McPherson (1994) using crystallographic techniques, showed that like the hexamer of soy glycinin, the edestin molecule is also composed of six identical subunits, and each subunit consists of AS and BS linked by one disulfide bond (Patel et al., 1994). Additionally, the lanes of reducing and non-reducing did not have significant differences, indicating there were not many disulfide bonds in the HPI structure.

The band at about 48.0 kDa was possibly hemp 7S vicilin-like protein, basically a 7S globulin, similar to the β-subunit of soybean β-conglycinin (Tang et al., 2006). A protein band below 20 kDa present in HPI was identified as albumin storage protein (Mamone et al., 2019).

In contrast, when HPI was dissolved in pH 4.0 acetate buffer (lane 2, 3), the bands for 7S vicilin-like protein, AS, and BS disappeared or became less intense. The peptides with low MW of less than 15 kDa were increased compared to HPI in water. Therefore, due to the decrease in pH, 7S vicilin-like protein, AS, and BS were harder to dissolve while low MW peptides became more soluble.

3.1.2 Particle size distribution of HPI and HPI-KC complexes

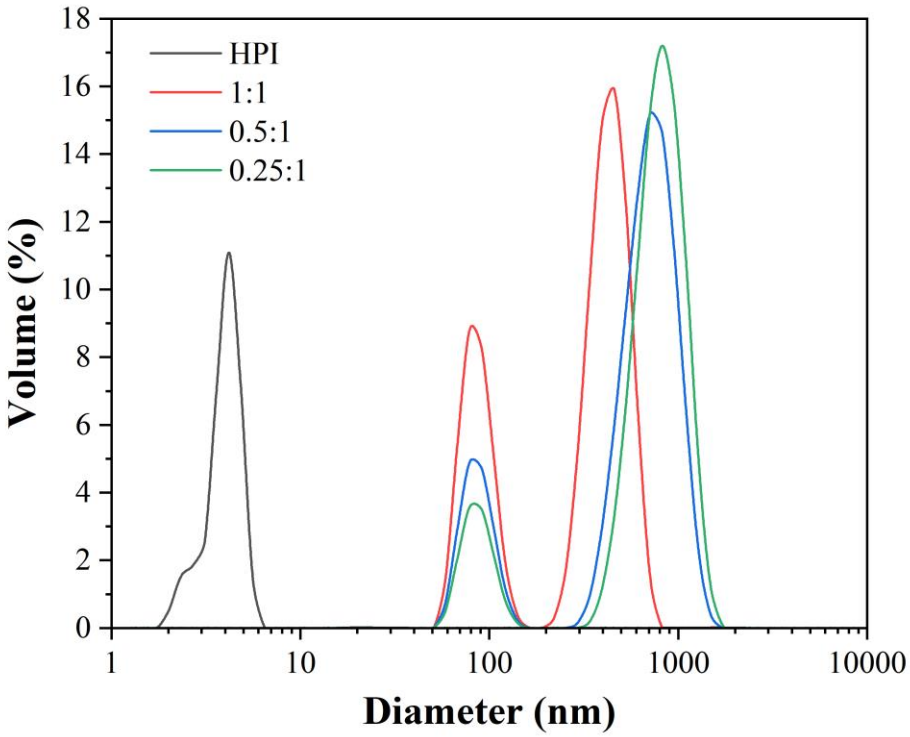

Fig.2. Particle size distributions of HPI and HPI-KC complexes at ratios of 1:1, 0.5:1 and 0.25:1 in acetate buffer (20 mM, pH 4.0). For clarity, one representative distribution is shown for each sample, but comparable distributions were obtained for at least three replicates.

The interfacial properties are significantly influenced by the size of particles or molecules, which dictates the diffusion rate towards the interface and the energy barrier for adsorption (Shen et al., 2023).

Therefore, particle size distributions (Fig.2) were measured to explore the influence of the ratio of HPI to KC on the overall particle sizes of their mixtures. The peak of HPI was between 2.0 – 5.6 nm with a maximum of 4.2 nm. When mixing HPI and KC, the maximum peaks at a ratio of 1:1, 0.5:1, and 0.25:1 were 459, 712, and 825 nm respectively, which was much larger than the particle size of HPI. This phenomenon suggests that HPI and KC could form larger electrostatic complexes during after mixing, which indicates that proteins can interact with polysaccharides through a variety of physical and chemical mechanisms, allowing them to assemble into structures that have new functions (Lima et al., 2023). When the content of KC increased, the particle size of complexes increased as well. Additionally, all HPI-KC complexes had a similar second-highest peak around 79 – 91 nm, and the peak became lower when the protein content of the complexes became lower. Therefore, these can be supposed to be the peaks for excess protein aggregates.

3.1.3 Zeta potential of HPI and HPI-KC complexes

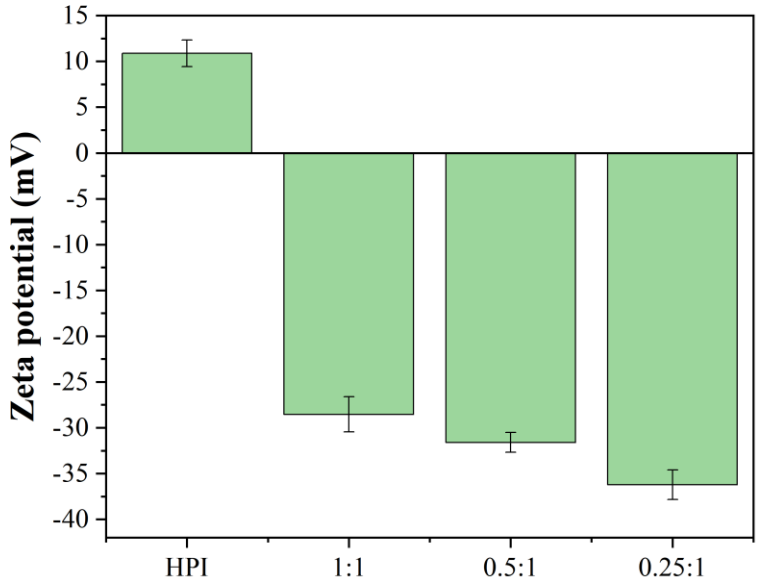

Fig.3. Zeta potential of HPI and HPI-KC complexes at ratios of 1:1, 0.5:1 and 0.25:1 in acetate buffer (20 mM, pH 4.0). The averages and standard deviations were the results of at least three replicates.

The formation of non-covalent electrostatic complexes between proteins and polysaccharides depends on the intrinsic properties of the macromolecules and on factors that influence these intrinsic properties,

such as pH, ionic strength, solvent quality, etc.

As shown in Fig.3, HPI represented a positive zeta potential at 10.9 mV. At pH 4.0, below the isoelectric point (pH 4.5-5) there was an abundance of protonated amino groups (-NH3+) compared to carboxyl groups (COO−), resulting in a net positive surface charge on the hemp protein (Gholivand et al., 2024). For HPI-KC complexes, because of adding polysaccharides, the zeta potential became negative. Comparing the net magnitude of the zeta potential , 1:1 complex showed the lowest of 28.5 mV while 0.25:1 showed the highest of 36.2 mV. Therefore, as the content of polysaccharides increased, the net magnitude of zeta potential became higher.

3.2 Interfacial dilatational rheology of HPI- and HPI-KC-stabilized oil-water interfaces

3.2.1 Interfacial adsorption behaviors of HPI and HPI-KC complexes

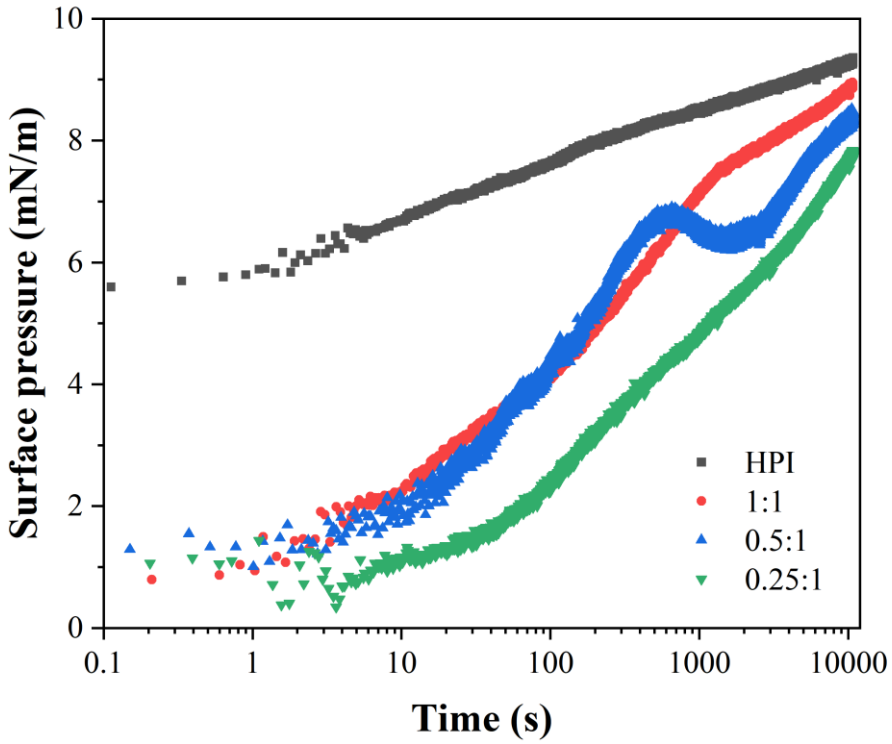

Fig.4. Surface pressure as a function of time studied using auto drop tensiometry (ADT) of HPI and HPI-KC complexes at a ratio of 1:1, 0.5:1, and 0.25:1. The protein concentration was 0.1 wt% in acetate buffer (20 mM,

pH 4.0). For clarity, one representative distribution is shown for each sample, but comparable distributions were obtained for at least three replicates.

The interfacial adsorption behaviors of HPI and HPI-KC complexes at a ratio of 1:1, 0.5:1, and 0.25:1 were measured between 0.1 and 10800 s by automatic drop tensiometer (ADT). The dynamic adsorption behavior of protein molecules at the oil-water interface mainly involves diffusion, actual adsorption (penetration and unfolding), and molecular rearrangement (T. Wang et al., 2023). The dynamic adsorption, infiltration, and rearrangement of proteins at the oil-water interface have an important impact on their emulsification properties and emulsification stability (Zhang et al., 2023).

The results in Fig.4 indicate that the presence of KC had a significant influence on the interfacial pressure generated by HPI adsorption at the oil-water interface. For HPI, the surface pressure reached 5.6 mN/m after 0.1 s, which was much higher than HPI-KC complexes of all ratios. For HPI-KC complexes, there were no significant differences for all ratios in the initial time between 0.1-1 s, which were all around 1.0 mN/m. The results clearly showed a faster diffusion of HPI to the oil-water interface than HPI-KC complexes in the initial time, possibly due to their smaller size and lower molecular weight making them able to diffuse faster towards the interface (Kontogiorgos & Prakash, 2023). Because HPI-KC complexes had larger particle sizes, they would have a slower diffusion rate towards the oil-water interface. Besides, this might also be due to HPI interacting with the KC that shields part of the hydrophobic groups of the protein on the surface, leading to lower surface activity (Zhang et al., 2023).

During the diffusion and adsorption between 1-10800 s, the surface pressure of HPI had a gently rising rate and was always higher than that of the complexes. After 10800 s, the surface pressure of HPI had reached 9.3 mN/m, higher than all complexes, which means smaller HPI particles can form a more densely packed interface (Yang et al., 2021). As for HPI-KC complexes of different ratios, all of them had a faster adsorption rate than HPI. This indicated that the complexes were gradually adsorbing to the surface. However, the surface pressure of HPI-KC complexes was still lower than HPI. After 10800 s, 1:1 complexes had higher surface pressure at 8.9 mN/m and 0.25:1 complexes had the lowest at 7.8 mN/m.

3.2.2 Frequency sweeps of HPI- and HPI-KC-formed oil-water interfaces

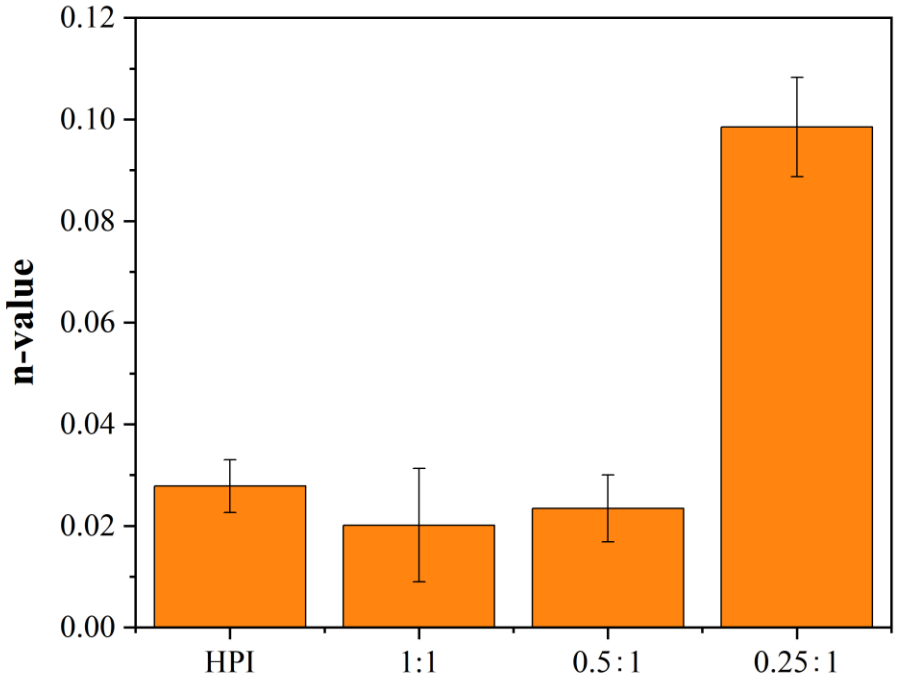

Fig.5. The value of the power-law exponent *n* obtained from the dilatational frequency sweeps for interfaces stabilized by HPI, HPI-KC complexes at a ratio of 1:1, 0.5:1, and 0.25:1. The averages and standard deviations were the results of at least three replicates.

In the frequency sweeps, n-values were calculated to assess the dominant mechanism in the surface stress response of the generated interfacial films. The n-values fell within the range of 0.020 to 0.099 (Fig.5), indicating a weak power-law trend, which is commonly observed in soft disordered solid materials (Shen et al., 2023).

A value of n = 0.5 would suggest that the elasticity of the interface is predominantly affected by the exchange of stabilizer between the bulk and interface (Lucassen & Van Den Tempel, 1972). Hence, the primary mechanism is not the exchange of material between the interface and bulk. Instead, other factors appear to exert greater influence, like in-plane interactions resulting from protein rearrangement at the interface or momentum transfer between the bulk and interface (L. M. C. Sagis et al., 2019). Additionally, the 0.25:1 complex exhibited a higher frequency dependency, indicating a more mobile

interface compared to others. This could indicate that the 0.25:1 stabilized interfaces had more exchange of materials between the bulk and interface, compared with other samples.

3.2.3 Amplitude sweeps of HPI- and HPI-KC-formed oil-water interfaces

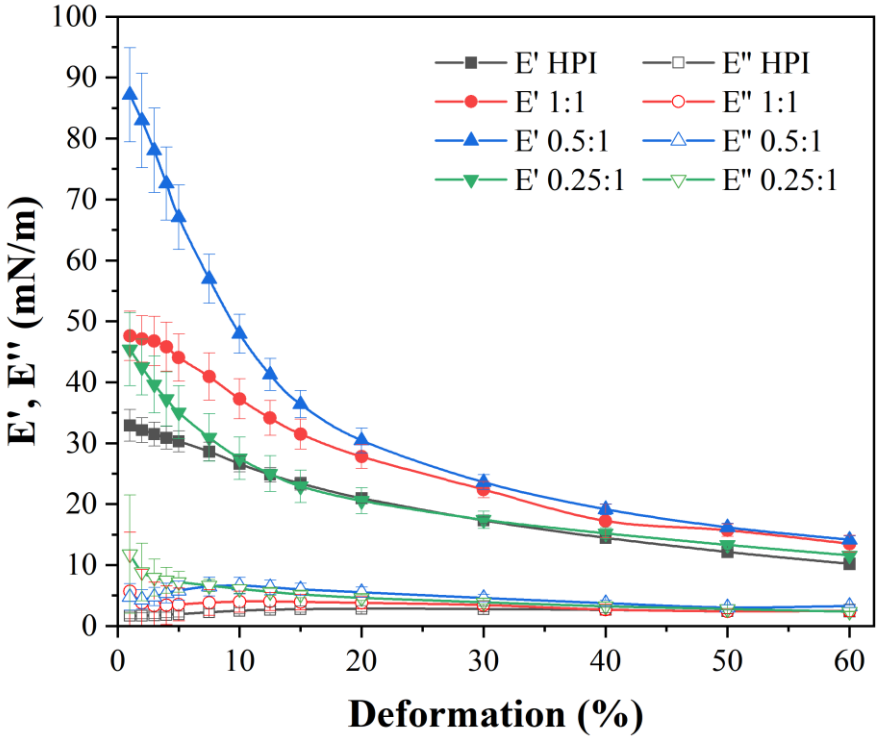

Fig.6. Interfacial dilatational storage (E_d') and loss (E_d'') moduli as a function of deformation amplitude at a fixed frequency of 0.02 Hz. The concentration of HPI and HPI-KC complexes was 0.1 wt% in acetate buffer (20 mM, pH 4.0). The averages and standard deviations were the results of at least three replicates.

Fig.6 shows the storage (E_d') and loss (E_d'') moduli of HPI and HPI-KC complexes during the amplitude sweeps. The E_d' expresses the amount of energy that is either recovered or stored in the material during each cycle of deformation. E_d'' measures the amount of energy lost by viscous dissipation in every cycle of deformation (Apostolidis et al., 2024). The loss tangent (tanδ) is a quantitative measure of the solid-like elastic or liquid-like viscous properties of the systems (Chae & Hong, 2011). All the HPI and HPI-KC complexes had higher storage moduli (E_d') than loss moduli (E_d'') during every amplitude, implying the tanδ (E_d''/E_d') < 1, which indicates that their interfacial films had solid-like rheological behavior in this deformation regime (Chae & Hong, 2011). Besides, these amplitude-dependent moduli also

suggested that the applied deformations were in the non-linear viscoelastic (NLVE) regime (Shen et al., 2023).

In the amplitude sweeps, the storage moduli of all HPI and HPI-KC interfacial films gradually decreased from the range of 32-87 mN/m to 10-14 mN/m with increasing amplitude, suggesting the increased structural disruption of these interfacial films (Yang et al., 2021). Storage moduli (E_d') of all HPI-KC complexes decreased faster than that of HPI, especially the 0.5:1 HPI-KC complex, decreasing from 87 mN/m to 14 mN/m, which indicates the interfacial films of all complexes had more severe structural disruption. The E_d' of HPI-KC complexes was always higher than that of HPI in the whole amplitude range, indicating the HPI-KC complexes formed a stiffer interface than HPI (Shen et al., 2023). Additionally, 0.5:1 HPI-KC complex had the highest E_d' during the whole amplitude range, which suggested that 0.5:1 HPI-KC complex formed the stiffest oil-water interface.

3.2.4 Lissajous plots for HPI- and HPI-KC-stabilized interfaces

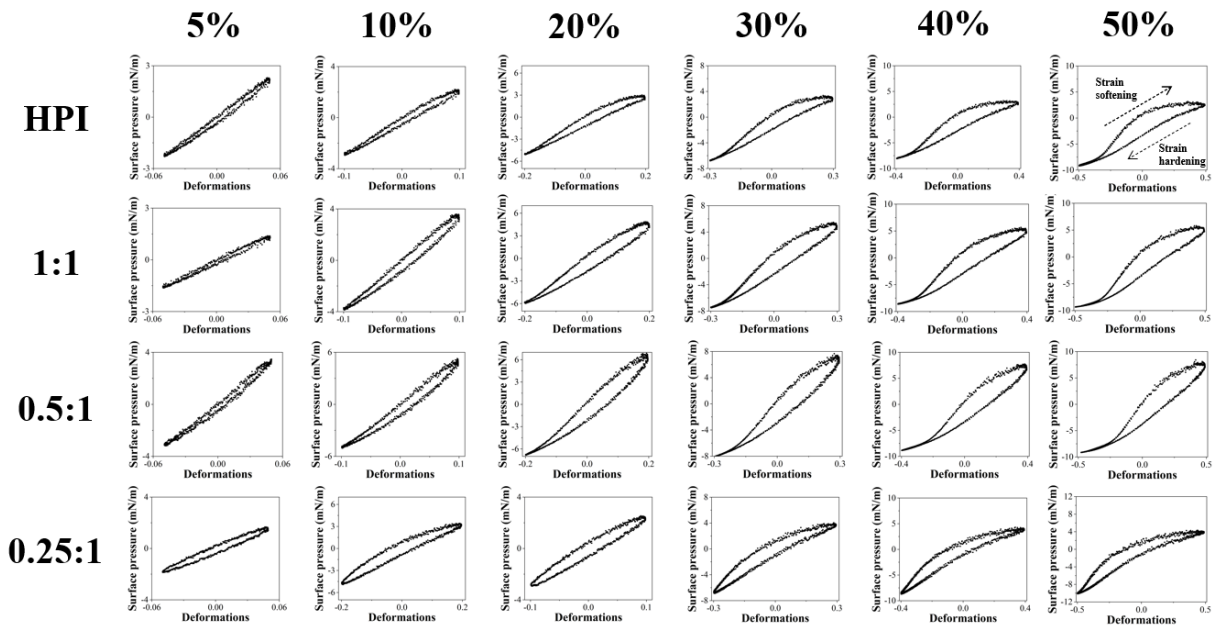

Fig.7. Lissajous plots of surface pressure as a function of the applied deformation, obtained from amplitude sweeps of oil-water interfacial films stabilized by HPI, HPI-KC complexes at a ratio of 1:1, 0.5:1 and 0.25:1. The deformation amplitude is indicated on the top row. For clarity, one representative plot is shown for each sample, but comparable plots were obtained on at least three replicates.

The stiffness of the interfacial layer is usually quantified within the linear regime (LVE) by calculating surface dilatational or shear moduli, which are calculated from the first-order harmonic from a Fourier transform of the stress signal. When the response enters the NLVE regime, higher harmonics are present in the stress response (even and odd ones in dilatation). Higher harmonics are completely neglected in the first harmonic moduli, but their contribution can be analyzed in Lissajous plots by plotting the interfacial stress directly versus the deformation (Yang et al., 2021).

The Lissajous plots in Fig.7 were highly asymmetrical, a typical feature for interfaces with a complex microstructure (L. M. C. Sagis & Scholten, 2014). In Lissajous plots, the surface stress changes in a clockwise direction with applied strain, where the upper part indicates the extension of the interface (from fully compressed to fully extended), and the lower part indicates the compression of the interface. A linear Lissajous plot represents a purely elastic response, a perfectly circular Lissajous plot represents a purely viscous response, and an elliptical Lissajous plot represents a linear viscoelastic response (Shen et al., 2023).

All Lissajous plots had a long and narrow shape at 5% deformation (Fig.7), which revealed a linear viscoelastic behavior, where the elastic component dominated the stress response. With increasing deformation to 50%, all Lissajous plots became asymmetric and wider, indicating the generation of non-linear responses and an increased contribution of the viscous component to the stress response due to the disruption of the interfacial microstructures (Yang et al., 2021).

For the HPI-stabilized interface, starting at the maximum compression at 50% deformation, there was a rapid increase in surface pressure, which indicated a predominantly elastic response. Upon further extension, the slope of the surface pressure curve gradually decreased. Around a deformation of 0.0, the rapid increase becomes more gradual and reaches a plateau where the slope is close to zero. This point depicts intra-cycle yielding, where the viscous contribution starts dominating, and the interfacial layer starts flowing (Yang et al., 2021). This phenomenon upon extension is called strain softening and is mainly due to the decrease of the protein density at the interface and the disruption of the interfacial

microstructure (Shen et al., 2023). The opposite phenomenon appeared upon compression (Fig.4), which is known as strain hardening. This phenomenon was attributed to the jamming of the interfacial fractured structures and the increased protein density at the interface (Yang et al., 2020).

For HPI-KC complexes, the Lissajous plots of 1:1 and 0.5:1 complex-stabilized interfaces were as wide as those of the HPI-stabilized interfaces. However, at the highest amplitude, they do not display a similarly abrupt yielding as the HPI-stabilized interfaces, but instead a more gradual strain softening. According to this phenomenon, the microstructure of the complex-stabilized interface is less disrupted by the applied deformation, which can be the result of the formation of a more stretchable network by complexes (Yang et al., 2020). The slope of the plot does not go to zero after yielding, which indicates that the interface retains a considerable degree of elasticity (Yang et al., 2020). In contrast, for 0.25:1 complex-stabilized interface, the Lissajous plot at 50% deformation showed an earlier initial increase followed by a sudden decrease to near-zero slope, indicating the elastic component in the response diminishes, and results in the flow of the system and more strain softening behavior (Yang et al., 2020). To further analyze the non-linear behaviors of these interfaces, the Lissajous plots were decomposed to separate the contributions of network disruption and surface density changes by a general stress decomposition (GSD) method.

3.2.5 General stress decomposition (GSD)

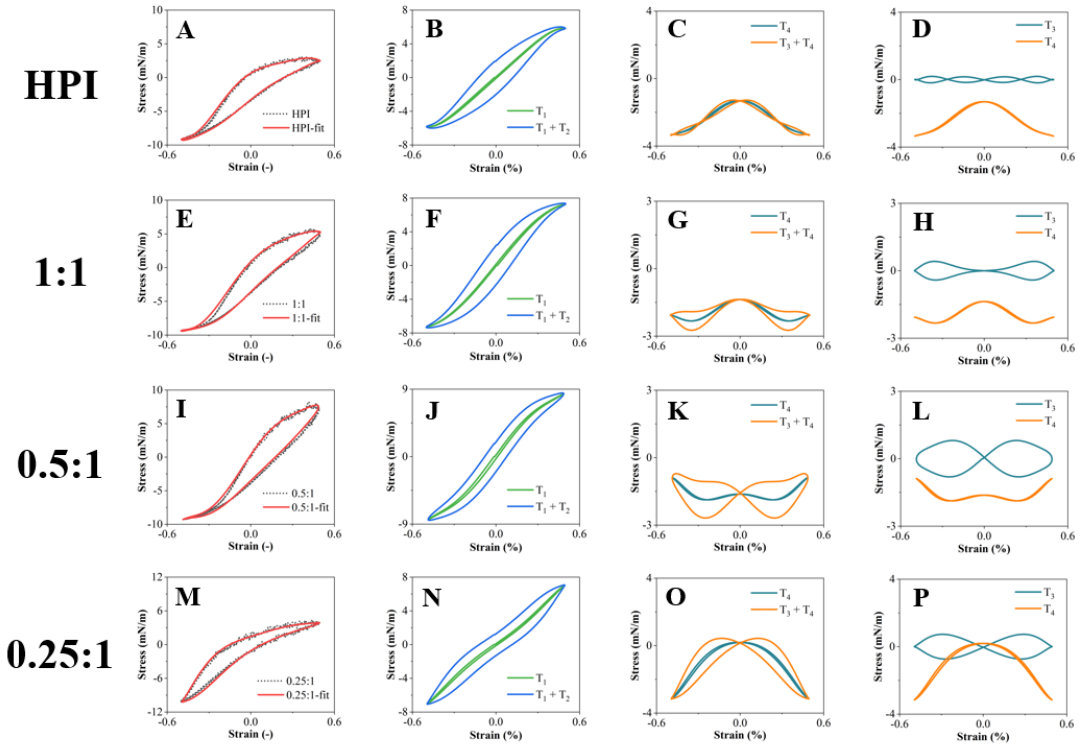

Fig.8. Lissajous plots of the surface pressure as a function with decomposed components τ1, τ2, τ3, τ4 of applied deformation (50%). The plots are obtained from amplitude sweeps (dilatational deformation) of oil-water interfacial films stabilized by HPI and HPI-KC complexes at a ratio of 1:1, 0.5:1, and 0.25:1 at pH 4.0. The samples were measured at least in triplicates, and one representative plot is shown.

The different responses observed in Lissajous plots (Fig.8) might arise from either network interactions or surface density changes. However, distinguishing between these two phenomena based only on the overall Lissajous plots is not feasible. Hence, the Lissajous plots were further decomposed using a general stress decomposition (GSD) method to separate the contributions from network disruption (odd harmonics) and surface density changes (even harmonics). Both contributions encompass an energy-storage element and an energy-dissipating component. Odd harmonics specifically include an elastic component (τ1) and a viscous component (τ2), while even harmonics consist of an energy-storing component (τ4) and a dissipating component (τ3) (de Groot et al., 2023).

For HPI- and HPI-KC-stabilized oil-water interfaces, asymmetric Lissajous plots were observed during large amplitude dilatation. The asymmetry suggests a notable presence of even harmonics during large

deformations (de Groot et al., 2023). For all the HPI- and HPI-KC-stabilized interfaces, the plots for τ1 + τ2 had minor hardening at maximum strain, which suggests a certain amount of network disruption had occurred in all interfaces. The fact that τ1 still had a finite slope around zero strain indicates only partial disruption of the microstructure (de Groot et al., 2023). Additionally, the 0.5:1 complex-stabilized interface had a slightly larger slope of τ1, which suggests a stronger interface.

According to Fig.8 C, D, G, H, K, L, O, P, in all HPI- and HPI-KC-stabilized interfaces, the even harmonics demonstrate a notable involvement of τ3 and τ4. τ4 of HPI and 0.25:1 complex were more negative than the others, suggesting their interfaces have a more pronounced contribution of surface density changes upon dilatational deformation (Yang et al., 2024). τ3 of 0.5:1 complexes had the widest loop, indicating a significant dissipative contribution in the even harmonics, which means that diffusional exchange may also be important in this sample. Analyzing through Lissajous plots for accurate comparison had posed certain challenges, therefore, quantification over the whole strain sweep, as shown in Fig.9, was required. Moreover, τ4 of all HPI- and HPI-KC-stabilized interfaces showed a vertical (negative) shift, and the average of τ4 was negative. This shift is an indication that we are oscillating around a non-equilibrium state and causes an overall shift of the total stress with respect to the horizontal axis (de Groot et al., 2023).

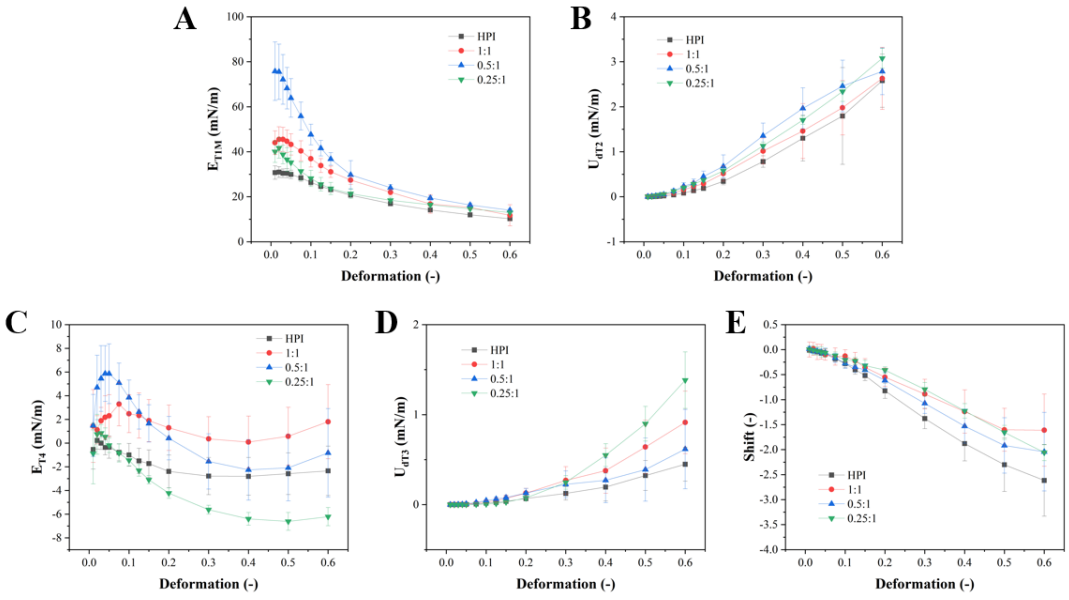

Fig.9. $E_{\tau 1M}$ (A), $U_{d\tau 2}$ (B), $E_{\tau 4}$ (C), $U_{d\tau 3}$ (D) and vertical shift (E) plotted over the range of deformations applied in the strain sweep for oil–water interfaces stabilized by HPI and HPI-KC complexes at a ratio of 1:1, 0.5:1 and

0.25:1 at pH 4.0. The samples were measured at least in triplicate, and the average and standard deviations are given in the figure.

Fig.9 quantified the contributions from τ1-τ4, based on their Fourier series, and showed how the introduced parameters can be visualized in the Lissajous plots. The slope of the curve for τ1 is a measure of the stiffness of the interfacial network and represents a (contribution to) dilatational storage modulus. To quantify intracycle strain stiffening, a modulus at zero deformation ($E_{\tau 1M}$) is defined, shown in Fig.9 A. It was shown that all $E_{\tau 1M}$ decreased during 0 – 0.6 deformation, indicating there was some structure disruptions in all interfaces at larger deformations. HPI-stabilized interfaces had a lower initial stiffness over the whole strain range compared to the HPI-KC samples, suggesting that HPI formed a weaker interface than other complex-stabilized interfaces. For HPI-KC, the 0.5:1 complex had the stiffest interface while the 0.25:1 complex had the weakest interface. The results confirm the observation in the Lissajous plots.

The dissipated energy in the loops of τ2 and τ3 ($U_{d\tau 2}$ and $U_{d\tau 3}$) (Fig.9 B, D) can also be calculated, which are equal to the total surface area enclosed by the stress versus strain plots (de Groot et al., 2023). It can be seen that for viscous energy dissipation $U_{d\tau 2}$, the 0.5:1 complex showed the highest energy dissipation during 0 – 0.5 deformation. This mainly because the 0.5:1 complex decreased the most in $E_{\tau 1M}$, which indicated more network disruption. The 0.25:1 complex also showed a high value of $U_{d\tau 2}$ and even exceeded the 0.5:1 complex at 0.6 deformations. This could indicate that there was high friction between particles, leading to high energy dissipation. In addition, HPI showed the lowest $U_{d\tau 2}$ energy dissipation. For $U_{d\tau 3}$, the 0.25:1 complex had the highest energy dissipation at large dilatation and HPI was the lowest. The results suggested a significant dissipative contribution in the even harmonics of the 0.25:1 complex and the nonlinearities in the Lissajous plots were more related to changes in surface density. This also confirmed the n-value results in Fig.4. Moreover, HPI exhibited the lowest values for the dissipated energy linked with τ2 and τ3, indicating weak network formation and suggesting restricted diffusional exchange during deformation. Therefore, HPI and 0.25:1 complexes may form jammed and glass-like interfaces, which was significantly weaker than the 0.5:1 and 1:1 complexes. In contrast, the 0.5:1 and 1:1 complexes may form more gel-like interfaces, which were more resistant to dilatational

deformation than HPI and 0.25:1 complexes.

If the elastic modulus $E_{\tau 4}$ (Fig.9 B) was increasingly negative, the phenomenon indicated a more significant contribution of surface density changes, due to (partially) irreversible absorption (on the timescale of a single oscillation cycle) (de Groot et al., 2023). However, at deformations > 0.3, τ4 showed an upturn at maximum compression, and expansion in interfaces stabilized by HPI and HPI-KC complexes showed an upward trend at deformations > 0.4. The upswing may have various implications, including a potential inflection point in the surface-pressure area isotherm or out-of-plane deformations such as interfacial buckling or the formation of compression-induced multilayers, which would result in a levelling-off of the plot towards maximum intracycle compression (Yang et al., 2024). Therefore, only $E_{\tau 4}$ at deformations ≤ 20% for all interfaces would be interpreted. As Fig.9 B showed, $E_{\tau 4}$ of HPI and 0.25:1 complex were negative on the average, which suggest a more significant contribution of surface density changes during dilatational deformation for HPI and the 0.25:1 complex, in contrast to other complexes.

Fig.9 E quantified the shift of τ4 from the 0^{th} harmonic of the Fourier series. HPI- and all the HPI-KC complex-stabilized interface showed obvious shift. Typically, in these experiments, after droplets form, the interface is initially allowed to approach a state of (near) equilibrium. After this initial phase, oscillations start upon reaching a quasi-equilibrium surface tension. The shift of τ4 implies that during oscillation, the system oscillates around a non-equilibrium state of the interface (de Groot et al., 2023). This shift was much higher for HPI than for the other complexes.

Overall, based on GSD, the 0.5:1 and 1:1 complexes formed stiffer oil-water interfaces than the 0.25:1 complexes and HPI in response to dilatational deformations. The former interfaces had more contributions from the in-plane network interactions, while the latter interfaces had more contributions from surface density change. Based on these, we can conclude that HPI and 0.25:1 complexes may form jammed and glass-like interfaces, which were significantly weaker than the 0.5:1 and 1:1 complexes. In contrast, the 0.5:1 and 1:1 complexes may form more gel-like interfaces, which were more resistant

to dilatational deformation than HPI and 0.25:1 complexes.

3.3 Characterization of HPI- and HPI-KC-stabilized emulsions

Emulsion stability refers to the ability of emulsions to resist changes in their physicochemical properties over time (Hu et al., 2017). Stable emulsions require the emulsifiers at the interface to prevent the recoalescence of oil droplets, which can be achieved through several mechanisms. One mechanism is the electrostatic repulsion between oil droplets. A higher charge of emulsifiers results in increased surface charge surrounding the oil droplets, potentially enhancing electrostatic repulsion, which prevents the flocculation and merging of newly formed oil droplets. Another factor to consider is the mechanical properties of the protein layer. A more rigid interfacial layer increases resistance against film rupture between two flocculated oil droplets. Additionally, a thicker interfacial layer may provide stronger steric repulsion (Yang et al., 2024). However, when using HPI-KC complexes as emulsifiers, insufficient polysaccharide concentrations or excessive amounts can lead to instability in the droplets, caused by either bridging or depletion flocculation. All these mechanisms could affect the long-term stability of emulsions significantly.

3.3.1 Emulsions microstructure

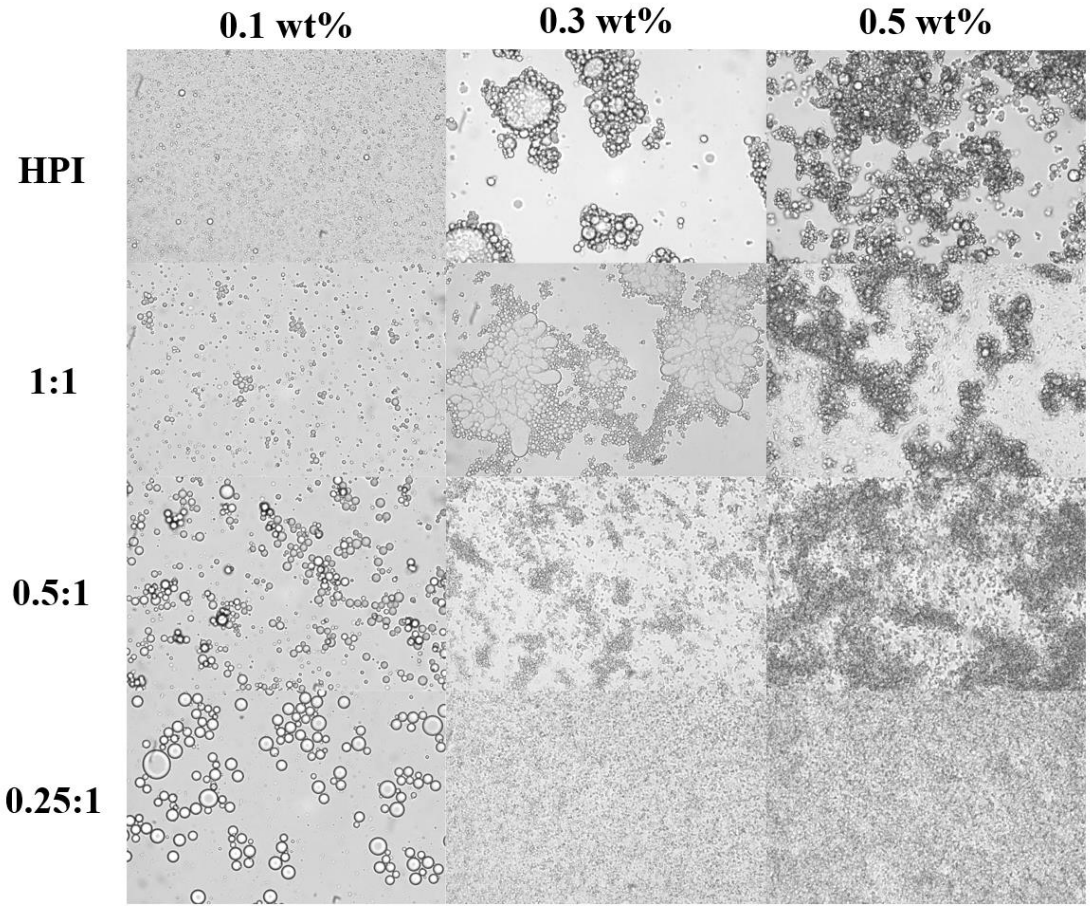

Fig.10. Micrographs of freshly prepared emulsions stabilized by HPI and HPI-KC complexes at ratios of 1:1, 0.5:1, and 0.25:1 at different concentrations of 0.1 wt%, 0.3 wt%, and 0.5 wt%.

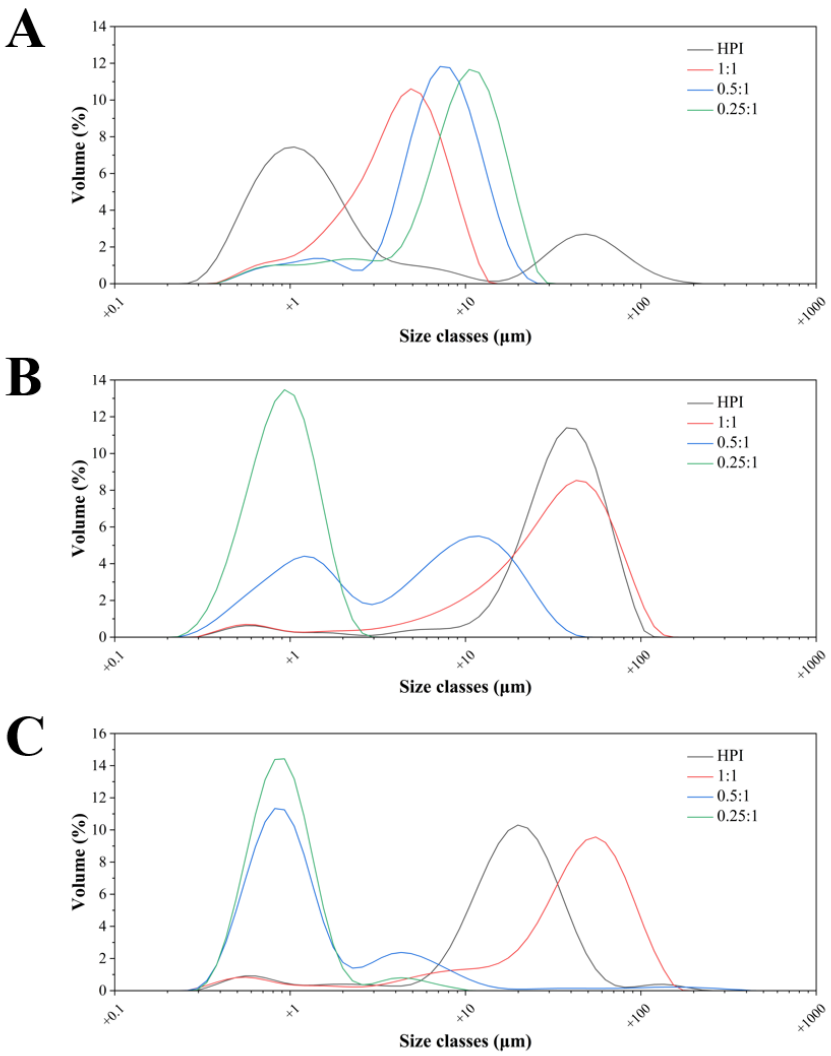

Fig.11. Particle size distribution of freshly prepared emulsions stabilized by HPI and HPI-KC complexes at ratios of 1:1, 0.5:1, and 0.25:1 at different concentrations of (A) 0.1 wt%, (B) 0.3 wt%, and (C) 0.5 wt%.

The dispersion levels and aggregation states of different freshly prepared emulsions can be clearly observed under the microscope (Fig.10). At 0.1 wt%, the oil droplets of HPI were the smallest and the most uniform, indicating the best dispersion level. For the complexes, as the ratio decreased, the oil droplets became larger. This may be because 0.1 wt% was too low and the HPI and HPI-KC particles were not enough to cover the interface of oil droplets (Tavernier et al., 2017). Therefore, as the protein content decreased, less complexes were formed, which resulted in more coalescence. However, at 0.3 wt% and 0.5 wt%, the phenomenon was quite the opposite. At both 0.3 wt% and 0.5 wt%, HPI-stabilized emulsions showed severe flocculation. This is mainly because the HPI exhibited relatively low hydrophilicity. For HPI-KC complexes, 1:1 complex-stabilized emulsions at both 0.3 wt% and 0.5 wt%

also had flocculation phenomenon. At the ratio of 0.5:1, the oil droplet size obviously became smaller, and the flocculation phenomenon is somewhat decreased but still partially present. However, at 0.25:1, both 0.3 wt% and 0.5 wt% emulsions demonstrated excellent stability with the smallest and uniform droplets, and no obvious flocculation was observed. These can also be confirmed by Fig.11. At 0.1 wt% (Fig.11 A), particle size became larger when the protein content decreased. At 0.3 wt% (Fig.11 B), 0.25:1 complex showed the smallest particle size. As for 0.5 wt% (Fig.11 C), both 0.5:1 and 0.25:1 complexes had the lowest particle size. Therefore, results above indicated that 0.25:1 complex formed the most stable emulsion. The different phenomenon above between different complex ratios were probably due to the thickness of the oil-water interface and repulsive forces (electrostatic repulsion). 0.25:1 complex had the highest absolute value of zeta potential (Fig.3), which could probably form a stronger electrostatic repulsion between oil droplets, leading to a better stability. In addition, a thicker interface may also be one of the reasons. Moreover, the degree of flocculation and coalescence of 0.3 wt% and 0.5 wt% cannot be decided only according to micrographs, so they will be discussed in the following part (3.3.2) as well.

3.3.2 Emulsifying stability

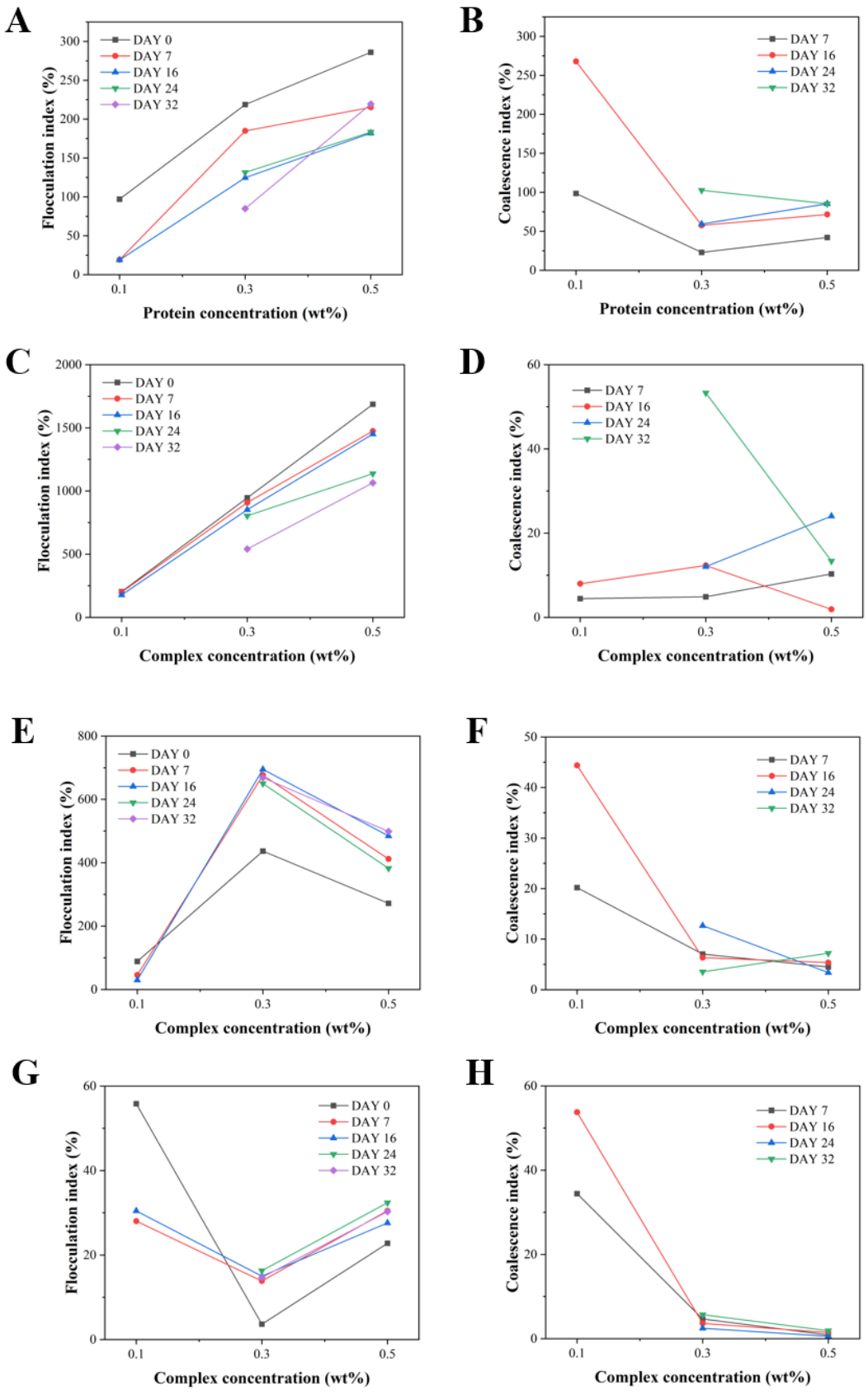

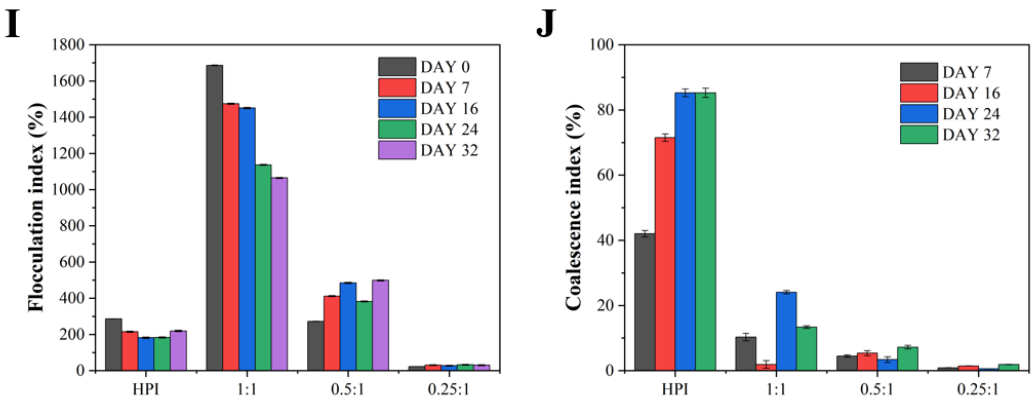

Fig.12. Flocculation and coalescence index of emulsions stabilized by HPI (A, B) and HPI-KC complexes at ratios of 1:1 (C, D), 0.5:1 (E, F) and 0.25:1 (G, H) at 0.1 wt%, 0.3 wt% and 0.5 wt% concentrations, and by HPI and HPI-KC complexes at ratios of 1:1, 0.5:1 and 0.25:1 at 0.5 wt% (I, J) during 32 storage days.

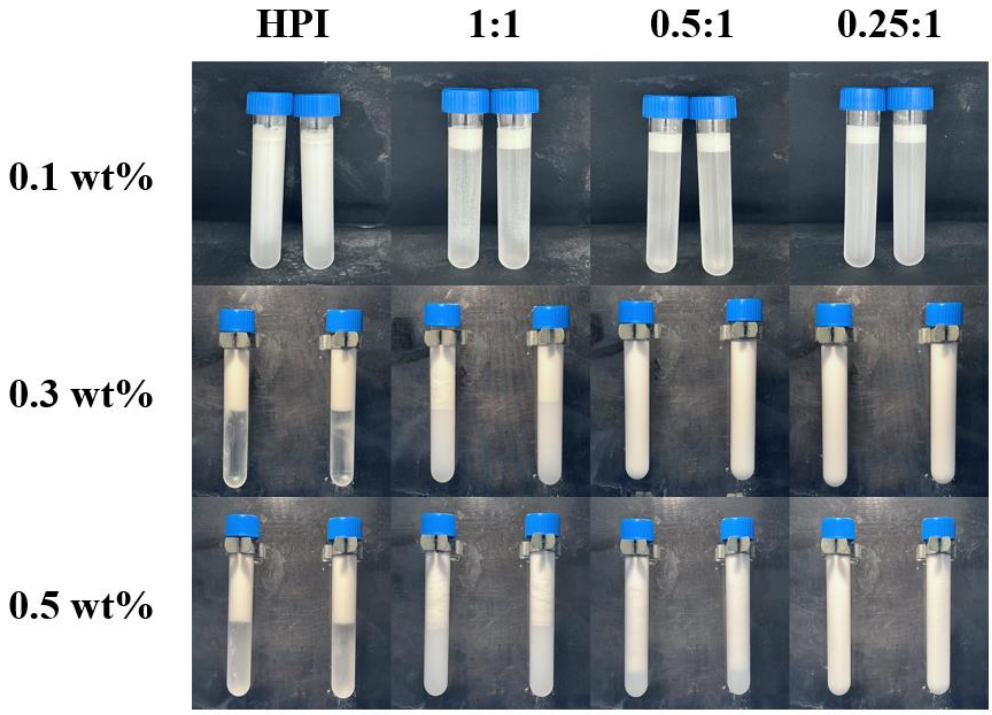

Fig.13. Macroscopic appearances of emulsions stabilized by HPI and HPI-KC in ratios of 1:1, 0.5:1 and 0.25:1 at 0.1 wt%, 0.3 wt% and 0.5 wt% concentrations after the storage time of 16, 32 and 32 days respectively.

The average droplet size of emulsions stabilized by HPI and HPI-KC complexes at ratios of 1:1, 0.5:1, and 0.25:1 at 0.1 wt%, 0.3 wt%, and 0.5 wt% concentrations was monitored during storage to evaluate the emulsifying stability. The volume-weighted average diameter, $D_{4,3}$ is more sensitive to the droplet size change than $D_{3,2}$ and is used to calculate the flocculation and coalescence indices for emulsions (Yang et al., 2024), as shown in Fig.12.

For HPI-stabilized emulsion, there was a pronouncedly increasing flocculation index with increasing protein concentration on the first storage day (Fig.12 A). During the storage time, the flocculation index became lower. The same phenomenon was also observed in 1:1 complex-stabilized emulsion (Fig.12 C). Besides, the coalescence index of HPI-stabilized emulsion became higher over time (Fig.12 B), which suggests that during the storage time, the flocculation finally turned into coalescence and led to the phase separation. As Fig.13 shows, HPI-stabilized emulsions all had obvious phase separation after storage days. For 1:1 complex-stabilized emulsion, the coalescence index did not present a significant trend (Fig.12 D). But it could be seen in Fig.13 that emulsions also showed phase separation, implying a certain amount of coalescence. Therefore, HPI- and 1:1 complex-stabilized emulsion did not exhibit both high coalescence stability during storage.

As for 0.5:1 complex-stabilized emulsion, the flocculation index of 0.3 wt% was the highest, and that of both 0.3 wt% and 0.5 wt% rose up within storage time (Fig.12 E). It was probably because most flocculation of 0.1 wt% emulsion turned to coalescence, as the highest coalescence index showed in Fig.12 F. Besides, due to the higher concentration, there might be more complexes adsorbed to the oil-water interface of 0.5 wt% emulsion, leading to higher electrostatic repulsion and steric repulsion and lower flocculation index. However, the coalescence index of both 0.3 wt% and 0.5 wt% emulsions maintained a low level during long-term storage (Fig.12 F), which indicated that they had high stability against coalescence. 0.25:1 complex-stabilized emulsion also provided the same coalescence stability of both 0.3 wt% and 0.5 wt% concentrations. Within the storage time, 0.3 wt% and 0.5 wt% of 0.25:1 complex-stabilized emulsion showed a rising flocculation index (Fig.12 G) while maintained a relatively low coalescence index (Fig.12 H). Additionally, the flocculation index of 0.5 wt% was higher than 0.3 wt%, which was the opposite of 0.5:1 emulsion. This may be because high polysaccharide content in 0.25:1 complex-stabilized emulsion resulted in depletion flocculation and therefore led to high flocculation index.

Comparison of the degree of flocculation index and coalescence index of 0.5 wt% emulsions were

shown in Fig.12 I, J. 1:1 complex-stabilized emulsion represented the highest flocculation index at the range of 1065% – 1686% while that of 0.25:1 complex-stabilized emulsion was much lower than all the others, around 23% - 32%. For the coalescence index, HPI-stabilized emulsion showed the highest degree compared to all complex-stabilized emulsions. During the storage time, the coalescence index of HPI-stabilized emulsion rose up from 42% to 85%. In contrast, 0.5:1 and 0.25:1 complex-stabilized emulsions represented a coalescence index lower than 10%. This phenomenon indicated that 0.5:1 and 0.25:1 complexes could clearly improve the coalescence stability of emulsions. This can also be confirmed by Fig.13. According to the pictures of 0.3 wt% and 0.5 wt% emulsions, after the long-term storage, HPI- and 1:1 complex-stabilized emulsions had obvious phase separation and 0.5:1 complex-stabilized emulsion broke slightly, while 0.25:1 complex-stabilized emulsion did not show macroscopic phase separation.

In summary, 0.5:1 and 0.25:1 emulsions exhibited better stability over long storage time. As the results of dilatation rheology showed, 0.5:1 complex-stabilized emulsion had the stiffest interface that could prevent oil droplets from coalescence which probably was the main reason why it maintained good emulsion stability over time. Moreover, 0.25:1 complex-stabilized emulsion showed the best flocculation and coalescence stability, which may be due to the higher charge of 0.25:1 complex (Fig.3) on the surface and led to higher electrostatic repulsion. Another possibility was that it formed a thicker interface and led to higher steric repulsion.

4. Conclusion

This study examined the role of HPI and HPI-KC complexes of different ratios (1:1, 0.5:1 and 0.25:1) in the stabilization of oil-water interfaces and the ability to stabilize emulsions. Dilatational rheology was used to explore the oil-water interface characteristics. At the initial time, HPI was faster to adsorb to the oil-water interface, may be due to its smallest particle size. Other complexes would adsorb to the interface gradually within 10,800 s. During the deformation periods, the 0.5:1 complex showed the highest E', suggesting a stiff interface. After turning the data into Lissajous plots and GSD, the results also demonstrated that 0.5:1 complex could create the stiffest and solid-like interfacial layers, exhibiting significant resistance to deformation. All HPI-KC complexes formed a more rigid interface than HPI, indicating the significant improvement in the oil-water interface stability of HPI-KC complexes. Among all the complexes, the 0.25:1 complex showed the most viscous interface. According to n-value and GSD, the nonlinearities in the Lissajous plots of HPI and 0.25:1 complex were more related to changes in surface density, while that of other complexes were more related to the interface structure breakdown.

Emulsions were made using HPI and HPI-KC complexes of different ratios (1:1, 0.5:1, and 0.25:1) at different concentrations (0.1%, 0.3%, and 0.5%) and stored for 16, 32, and 32 days respectively to observe emulsion stability. In micrographs of freshly prepared emulsions, 0.5:1 and 0.25:1 complex-stabilized emulsions at both 0.3 wt% and 0.5 wt% showed the smallest oil droplets, and 0.25:1 complex had the best dispersion. The particle size distribution also showed that 0.25:1 complex-stabilized emulsion had the smallest particle size at both 0.3 wt% and 0.5 wt%. After the long-term storage, the flocculation index of both HPI- and 1:1 complex-stabilized emulsions decreased while the coalescence index rose up, suggesting more flocculation turned into coalescence and led to phase separation. For 0.5:1 and 0.25:1 complex-stabilized emulsions at 0.3 wt% and 0.5 wt%, the flocculation index increased, but the coalescence index remained at low levels, indicating their better stability against coalescence. For 0.5:1 complex-stabilized emulsion, the main reason would be it formed a stiff interface, as the dilatation rheology data showed. For 0.25:1 complex-stabilized emulsion, the good stability may be due to the higher charge of 0.25:1 complex on the surface, and led to higher electrostatic repulsion. Another possibility was that it formed a thicker interface and led to higher steric repulsion.

The results of this study will provide deeper insights and useful information for improving the effectiveness of plant protein emulsifiers in making stable emulsions, which will help people better understand which foods could benefit from using them.

5. Reference

Apostolidis, E., Gerogianni, A., Anagnostaki, E., Paximada, P., & Mandala, I. (2024). Assembly of spherical-shaped resistant starch nanoparticles to the oil droplet surface promotes the formation of stable oil in water Pickering emulsions. *Food Hydrocolloids*, *151*. https://doi.org/10.1016/j.foodhyd.2024.109775

Chae, D. W., & Hong, S. M. (2011). Rheology, crystallization behavior under shear, and resultant morphology of PVDF/multiwalled carbon nanotube composites. *Macromolecular Research*, *19*(4), 326–331. https://doi.org/10.1007/s13233-011-0403-1

Chassenieux, C., & Nicolai, T. (2023). Mechanical properties and microstructure of (emul)gels formed by mixtures of proteins and polysaccharides. *Current Opinion in Colloid & Interface Science*, 101781. https://doi.org/10.1016/j.cocis.2023.101781

Cheng, J., Ma, Y., Li, X., Yan, T., & Cui, J. (2015). Effects of milk protein-polysaccharide interactions on the stability ofice cream mix model systems. *Food Hydrocolloids*, *45*, 327–336. https://doi.org/10.1016/j.foodhyd.2014.11.027

Day, L., Cakebread, J. A., & Loveday, S. M. (2022). Food proteins from animals and plants: Differences in the nutritional and functional properties. In *Trends in Food Science and Technology* (Vol. 119, pp. 428–442). Elsevier Ltd. https://doi.org/10.1016/j.tifs.2021.12.020

de Groot, A., Yang, J., & Sagis, L. M. C. (2023). Surface stress decomposition in large amplitude oscillatory interfacial dilatation of complex interfaces. *Journal of Colloid and Interface Science*, *638*, 569–581. https://doi.org/10.1016/j.jcis.2023.02.007

Do, D. T., Ye, A., Singh, H., & Acevedo-Fani, A. (2024). Protein bodies from hemp seeds: Isolation, microstructure and physicochemical characterisation. *Food Hydrocolloids*, *149*. https://doi.org/10.1016/j.foodhyd.2023.109597

Gholivand, S., Tan, T. B., Mat Yusoff, M., Choy, H. W., Teow, S. J., Wang, Y., Liu, Y., & Tan, C. P. (2024). Elucidation of synergistic interactions between anionic polysaccharides and hemp seed protein isolate and their functionalities in stabilizing the hemp seed oil-based nanoemulsion. *Food Hydrocolloids*, *146*. https://doi.org/10.1016/j.foodhyd.2023.109181

Hu, Y. T., Ting, Y., Hu, J. Y., & Hsieh, S. C. (2017). Techniques and methods to study functional characteristics of emulsion systems. In *Journal of Food and Drug Analysis* (Vol. 25, Issue 1, pp. 16–26). Elsevier Taiwan LLC. https://doi.org/10.1016/j.jfda.2016.10.021

Julakanti, S., Charles, A. P. R., Zhao, J., Bullock, F., Syed, R., Myles, Y., & Wu, Y. (2023). Hempseed protein (Cannabis sativa L.): Influence of extraction pH and ball milling on physicochemical and functional properties. *Food Hydrocolloids*, *143*. https://doi.org/10.1016/j.foodhyd.2023.108835

Karabulut, G., Kapoor, R., Yemis, O., & Feng, H. (2024). Manothermosonication, high-pressure homogenization, and their combinations with pH-shifting improve the techno-functionality and digestibility of hemp protein. *Food Hydrocolloids*, *150*. https://doi.org/10.1016/j.foodhyd.2023.109661

Kontogiorgos, V., & Prakash, S. (2023). Adsorption kinetics and dilatational rheology of plant protein concentrates at the air- and oil-water interfaces. *Food Hydrocolloids*, *138*. https://doi.org/10.1016/j.foodhyd.2023.108486

Li, X., Chen, X., & Cheng, H. (2024). Impact of κ-Carrageenan on the Cold-Set Pea Protein Isolate Emulsion-Filled Gels: Mechanical Property, Microstructure, and In Vitro Digestive Behavior. *Foods*, *13*(3). https://doi.org/10.3390/foods13030483

Lima, R. R., Stephani, R., Perrone, Í. T., & de Carvalho, A. F. (2023). Plant-based proteins: A review of factors modifying the protein structure and affecting emulsifying properties. In *Food Chemistry Advances* (Vol. 3). Elsevier Ltd. https://doi.org/10.1016/j.focha.2023.100397

Lucassen, J., & Van Den Tempel, M. (1972). Dynamic measurements of dilational properties of a liquid interface. In *Chemical Engineering Science* (Vol. 27). Pergamon Press.

Mamone, G., Picariello, G., Ramondo, A., Nicolai, M. A., & Ferranti, P. (2019). Production, digestibility and allergenicity of hemp (Cannabis sativa L.) protein isolates. *Food Research International*, *115*, 562–571. https://doi.org/10.1016/j.foodres.2018.09.017

McClements, D. J., Bai, L., & Chung, C. (2017). Recent Advances in the Utilization of Natural Emulsifiers to Form and Stabilize Emulsions. In *Annual Review of Food Science and Technology* (Vol. 8, pp. 205–236). Annual Reviews Inc. https://doi.org/10.1146/annurev-food-030216-030154

Patel, S., Cudney, R., & Mcpherson, A. (1994). Crystallographic Characterization and Molecular Symmetry of Edestin, a Legumin from Hemp. In *Mol. Biol* (Vol. 235).

Rawal, K., Annamalai, P. K., Ningtyas, D. W., & Prakash, S. (2024). Enhancement of emulsion stability and functional properties of hemp protein-based dairy alternative by different treatments after cellulase hydrolysis. *International Journal of Food Science and Technology*, *59*(1), 639–648. https://doi.org/10.1111/ijfs.16735

Sagis, L. M. C., Liu, B., Li, Y., Essers, J., Yang, J., Moghimikheirabadi, A., Hinderink, E., Berton-Carabin, C., & Schroen, K. (2019). Dynamic heterogeneity in complex interfaces of soft interface-dominated materials. *Scientific Reports*, *9*(1). https://doi.org/10.1038/s41598-019-39761-7

Sagis, L. M. C., & Scholten, E. (2014). Complex interfaces in food: Structure and mechanical properties. In *Trends in Food Science and Technology* (Vol. 37, Issue 1, pp. 59–71). Elsevier Ltd. https://doi.org/10.1016/j.tifs.2014.02.009

Sagis, L. M., & Yang, J. (2022). Protein-stabilized interfaces in multiphase food: comparing structure-function relations of plant-based and animal-based proteins. In *Current Opinion in Food Science* (Vol. 43, pp. 53–60). Elsevier Ltd. https://doi.org/10.1016/j.cofs.2021.11.003

Shen, P., Yang, J., Nikiforidis, C. V., Mocking-Bode, H. C. M., & Sagis, L. M. C. (2023). Cruciferin versus napin – Air-water interface and foam stabilizing properties of rapeseed storage proteins. *Food Hydrocolloids*, *136*. https://doi.org/10.1016/j.foodhyd.2022.108300

Tang, C. H., Ten, Z., Wang, X. S., & Yang, X. Q. (2006). Physicochemical and functional properties of hemp (Cannabis sativa L.) protein isolate. *Journal of Agricultural and Food Chemistry*, *54*(23), 8945–8950. https://doi.org/10.1021/jf0619176

Tavernier, I., Patel, A. R., Van der Meeren, P., & Dewettinck, K. (2017). Emulsion-templated liquid oil structuring with soy protein and soy protein: κ-carrageenan complexes. *Food Hydrocolloids*, *65*, 107–120. https://doi.org/10.1016/j.foodhyd.2016.11.008

Wang, N., Liu, B., Wang, D., Xing, K., Wang, W., Wang, T., & Yu, D. (2024). Oil-in-water and oleogel-in-water emulsion encapsulate with hemp seed oil containing Δ9-tetrahydrocannabinol and cannabinol: Stability, degradation and in vitro simulation characteristics. *Food Chemistry*, *444*. https://doi.org/10.1016/j.foodchem.2024.138633

Wang, T., Wang, N., Dai, Y., Yu, D., & Cheng, J. (2023). Interfacial adsorption properties, rheological properties and oxidation kinetics of oleogel-in-water emulsion stabilized by hemp seed protein. *Food Hydrocolloids*, *137*. https://doi.org/10.1016/j.foodhyd.2022.108402

Wang, X. S., Tang, C. H., Yang, X. Q., & Gao, W. R. (2008). Characterization, amino acid composition and in vitro digestibility of hemp (Cannabis sativa L.) proteins. *Food Chemistry*, *107*(1), 11–18. https://doi.org/10.1016/j.foodchem.2007.06.064

Yang, J., Shen, P., de Groot, A., Mocking-Bode, H. C. M., Nikiforidis, C. V., & Sagis, L. M. C. (2024). Oil-water interface and emulsion stabilising properties of rapeseed proteins napin and cruciferin studied by nonlinear surface rheology. *Journal of Colloid and Interface Science*, *662*, 192–207. https://doi.org/10.1016/j.jcis.2024.02.030

Yang, J., Thielen, I., Berton-Carabin, C. C., van der Linden, E., & Sagis, L. M. C. (2020). Nonlinear interfacial rheology and atomic force microscopy of air-water interfaces stabilized by whey protein beads and their constituents. *Food Hydrocolloids*, *101*. https://doi.org/10.1016/j.foodhyd.2019.105466

Yang, J., Waardenburg, L. C., Berton-Carabin, C. C., Nikiforidis, C. V., van der Linden, E., & Sagis, L. M. C. (2021). Air-water interfacial behaviour of whey protein and rapeseed oleosome mixtures. *Journal of Colloid and Interface Science*, *602*, 207–221. https://doi.org/10.1016/j.jcis.2021.05.172

Zhang, J., Xu, D., & Cao, Y. (2023). Physical stability, microstructure and interfacial properties of solid-oil-in-water (S/O/W) emulsions stabilized by sodium caseinate/xanthan gum complexes. *Food Research International*, *164*. https://doi.org/10.1016/j.foodres.2022.112370